

**Defect structures in  $B_{12}As_2$  epitaxial layers grown on (0001) 6H-SiC**H. Chen,<sup>1,a)</sup> G. Wang,<sup>1</sup> M. Dudley,<sup>1</sup> L. Zhang,<sup>2</sup> L. Wu,<sup>2</sup> Y. Zhu,<sup>2</sup> Z. Xu,<sup>3</sup> J. H. Edgar,<sup>3</sup> and M. Kuball<sup>4</sup><sup>1</sup>*Department of Materials Science and Engineering, Stony Brook University, Stony Brook, New York 11794, USA*<sup>2</sup>*Center for Functional Materials, Brookhaven National Laboratory, Upton, New York 11973, USA*<sup>3</sup>*Department of Chemical Engineering, Kansas State University, Manhattan, Kansas 66506, USA*<sup>4</sup>*H.H. Wills Physics Laboratory, University of Bristol, Bristol BS8 1TL, United Kingdom*

(Received 1 February 2008; accepted 11 April 2008; published online 17 June 2008)

A detailed analysis of the microstructure in  $B_{12}As_2$  epitaxial layers grown by chemical-vapor deposition on (0001) 6H-SiC substrates is presented. Synchrotron white beam x-ray topography enabled macroscopic characterization of the substrate/epilayer ensembles and revealed the presence of a quite homogeneous solid solution of twin and matrix epilayer domains forming a submicron mosaic structure. The basic epitaxial relationship was found to be  $(0001)_{B_{12}As_2} \langle 11\bar{2}0 \rangle_{B_{12}As_2} \parallel (0001)_{6H-SiC} \langle 11\bar{2}0 \rangle_{6H-SiC}$  and the twin relationship comprised a  $180^\circ$  (or equivalently  $60^\circ$ ) rotation about  $[0001]_{B_{12}As_2}$  in agreement with previous reports. Cross-sectional high resolution transmission electron microscopy revealed the presence of a  $\sim 200$  nm thick disordered transition layer which was shown to be created by the coalescence of a mosaic of translationally and rotationally variant domains nucleated at various types of nucleation sites available on the (0001) 6H-SiC surface. In this transition layer, competition between the growth of the various domains is mediated in part by the energy of the boundaries created between them as they coalesce. Boundaries between translationally variant domains are shown to have unfavorable bonding configurations and hence high-energy. These high-energy boundaries can be eliminated during mutual overgrowth by the generation of a  $1/3[0001]_{B_{12}As_2}$  Frank partial dislocation which effectively eliminates the translational variants. This leads to an overall improvement in film quality beyond thicknesses of  $\sim 200$  nm as the translational variants grow out leaving only the twin variants. (0003) twin boundaries in the regions beyond 200 nm are shown to possess fault vectors such as  $1/6[1\bar{1}00]_{B_{12}As_2}$ , which are shown to originate from the mutual shift between the nucleation sites of the respective domains. © 2008 American Institute of Physics. [DOI: 10.1063/1.2940132]

**I. INTRODUCTION**

Icosahedral borides with a rhombohedral structure are of interest due to their unusual bonding (two electrons shared by three atoms) and the associated self-healing resistance to radiation damage.  $B_{12}As_2$  is a semiconductor member of the icosahedral boride family based on clusters of boron atoms and two-atom As-As chains as shown in Fig. 1. It has a wide band-gap of 3.47 eV and is potentially useful for devices operating in high electron radiation environments.<sup>1-6</sup> A unique potential application of  $B_{12}As_2$  is for the beta cell, a device capable of directly producing electrical energy by coupling a radioactive beta emitter to a rectifying semiconductor junction.<sup>7,8</sup>

The current absence of native substrates of  $B_{12}As_2$  necessitates the growth of films by heteroepitaxy on lattice matched substrates. Epitaxial growth on 6H-SiC is facilitated since the in-plane lattice parameters of (0001) 6H-SiC are approximately one half those of (0001)  $B_{12}As_2$ , and there are a number of reports of epitaxial films grown on such substrates.<sup>1,7-9</sup> For films grown on  $3.5^\circ$  off-axis and on-axis (0001) 6H-SiC. Wang *et al.*<sup>7</sup> observed polycrystalline grains with preferred orientation of  $[0001]_{B_{12}As_2} // [0001]_{6H-SiC}$  and

$[10\bar{1}0]_{B_{12}As_2} // [10\bar{1}0]_{6H-SiC}$  to within  $3^\circ$ . Vetter *et al.*<sup>8</sup> confirmed this orientation relationship for films grown on on-axis substrates, although double positioning twins were also observed with one occurring more frequently than the other. Nagarajan *et al.*<sup>9</sup> found that the distribution of double positioning twins varied with different  $AsH_3:B_2H_6$  flow ratios. Michael *et al.*<sup>1</sup> theoretically predicted the existence of a number of possible  $B_{12}As_2$  structural variants based on the variety of nonequivalent nucleation sites available on the (0001) SiC surface. These were referred to as chemical, translational, and rotational variants although this analysis did not take into account the influence of the possible bonding configurations between the  $B_{12}As_2$  and SiC surface, a subject which we will address later. Double positioning twins were observed but no evidence was found for any preferred growth. Diffuse boundaries observed within the twin grains were tentatively interpreted as boundaries between translational variants. In addition, a boron carbide reaction layer was observed between the  $B_{12}As_2$  layer and the 6H-SiC substrate.

None of these earlier reports provide a detailed atomic level study of defect structures in  $B_{12}As_2$  on 6H-SiC. In the present work, we report such a study involving the combined use of synchrotron white beam x-ray topography (SWBXT)

<sup>a)</sup>Electronic mail: huichen@ic.sunysb.edu.

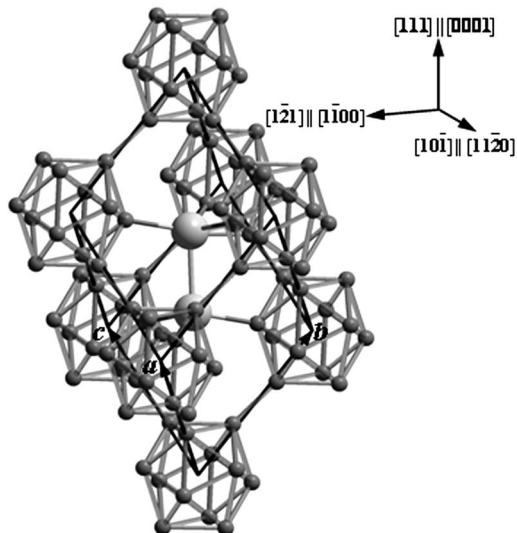


FIG. 1. View of  $B_{12}As_2$  unit cell showing boron icosahedra (B atoms are the smaller spheres) and an As–As chain (As atoms are the larger spheres). The structure can be equivalently referred to as either a rhombohedral or hexagonal unit cell.  $a$ ,  $b$ , and  $c$  indicate the rhombohedral unit cell axes. The  $[111]$ ,  $[1\bar{2}1]$ , and  $[10\bar{1}]$  directions indicated, referred to the rhombohedral cell, are equivalent to  $[0001]$ ,  $[1\bar{1}00]$ , and  $[11\bar{2}0]$ , respectively, in the hexagonal cell.

and high resolution transmission electron microscopy (HRTEM). Based on the HRTEM results, it is clearly shown that, for growth on either Si or C-face SiC, consideration of the possible bonding configurations at the interface precludes the existence of the chemical variants and places restrictions on the number of translational and rotational variants. The observed evolution of the film microstructure from a disordered mosaic transition layer comprising translational and rotational variants to a more ordered structure comprising only the rotational variants is explained based on the consideration of possible bonding configurations during coalescence between islands nucleated on the various nucleation sites.

## II. EXPERIMENT

$(0001)$  6H-SiC substrates were used for the chemical-vapor deposition (CVD) growth of  $B_{12}As_2$ . The  $B_{12}As_2$  films

were synthesized with gaseous precursors of 1%  $B_2H_6$  in  $H_2$  and 2%  $AsH_3$  in  $H_2$ . The films were deposited at 1450 °C and 100 Torr of reactor pressure for 30 min. The rhombohedral epitaxial films of  $B_{12}As_2$  had a nominal thickness of 3  $\mu\text{m}$ . The cross-sectional transmission electron microscopy (TEM) samples were made parallel to  $(11\bar{2}0)_{6H\text{-SiC}}$ , which is parallel to  $(11\bar{2}0)_{B_{12}As_2}$ , since this orientation clearly reveals the  $B_{12}As_2$  twin boundaries. Note that indices referenced to the four index hexagonal system are utilized throughout this paper. These can easily be related to the three index rhombohedral system using the standard relationship such that  $(11\bar{2}0)_{B_{12}As_2}$  is parallel to  $[10\bar{1}]_{B_{12}As_2}$ ,  $[0001]_{B_{12}As_2}$  is parallel to  $[111]_{B_{12}As_2}$ , and  $(0003)_{B_{12}As_2}$  is equivalent to  $(111)_{B_{12}As_2}$  (see Fig. 1). The sample was mechanically thinned and polished using the standard T-tool technique employing 30, 15, 6, 3, 1, and 0.5  $\mu\text{m}$  diamond lapping films and then ion milled to electron transparency. Conventional TEM observation was performed on a Philips CM12 transmission electron microscope with an accelerating voltage of 120 keV. HRTEM was carried out using a JEOL 3000EX system with an electron voltage of 300 keV. SWBXT was performed on as-grown films at the Stony Brook synchrotron topography facility at the National Synchrotron Light Source. The Laue patterns were recorded on Kodak SR5 x-ray films at a sample to a film distance of 15 cm. Structural projections were produced using the commercial software package CARINE 4.0.

## III. RESULTS AND DISCUSSION

Figure 2(a) shows a transmission synchrotron x-ray Laue pattern from the  $B_{12}As_2$  epitaxial layer grown on the  $c$ -plane 6H-SiC substrate recorded with the epilayer as the x-ray exit surface. The  $B_{12}As_2$  produced diffuse diffraction spots and detailed indexing analysis not only confirms the expected  $(0001)_{B_{12}As_2}\langle 11\bar{2}0 \rangle_{B_{12}As_2} \parallel (0001)_{6H\text{-SiC}}\langle 11\bar{2}0 \rangle_{6H\text{-SiC}}$  in an epitaxial relationship<sup>1,7,8</sup> but also shows that the  $B_{12}As_2$  is present in two distinct orientations related by a 180° twin or equivalently 60° rotation about the  $(0001)_{B_{12}As_2}$  plane normal. The strong, well-defined 6H-SiC diffraction spots are labeled with hexagonal  $hkil$  indices without subscripts, while

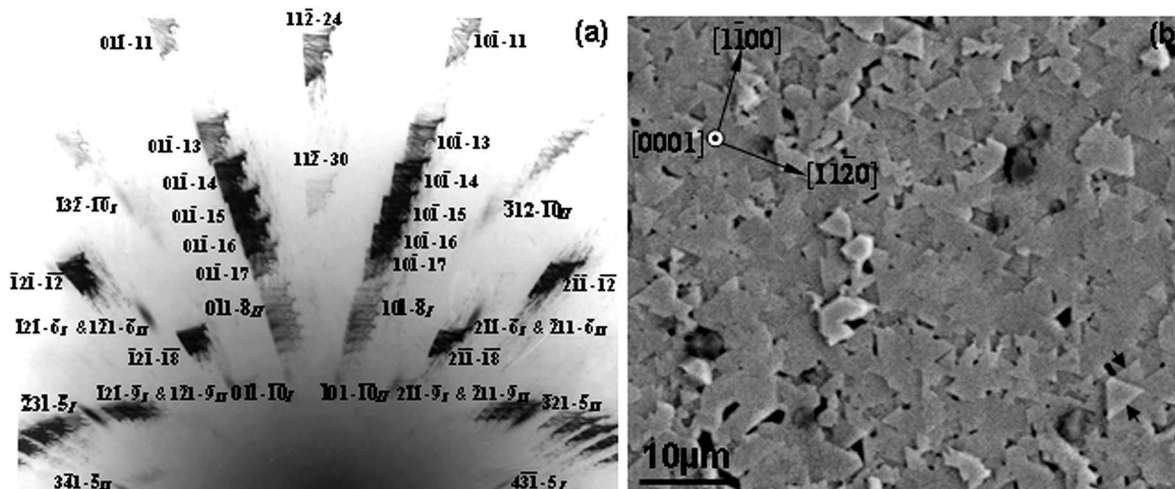


FIG. 2. (a) Indexed SWBXT Laue pattern recorded from the  $B_{12}As_2$  film grown on the  $c$ -plane 6H-SiC substrate. (b) SEM image showing the surface morphology of the  $B_{12}As_2$  film.

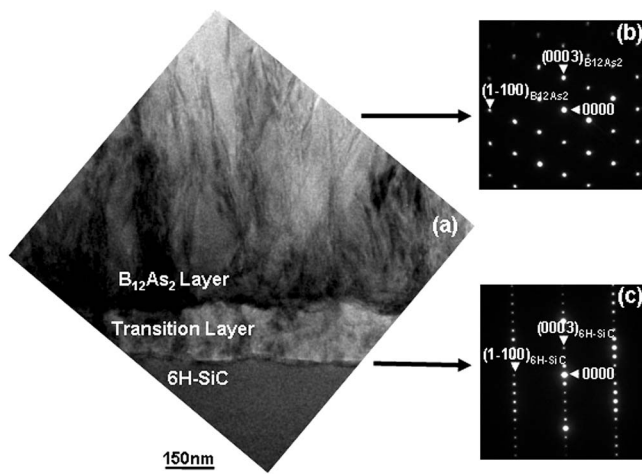


FIG. 3. (a) Cross-sectional TEM image recorded along  $[11\bar{2}0]$  revealing a transition layer located between the  $B_{12}As_2$  layer and the  $6H$ -SiC substrate. (b) SAD pattern of the  $B_{12}As_2$  epilayer recorded along the  $[11\bar{2}0]$  zone axis. (c) SAD pattern of the  $6H$ -SiC substrate recorded along the  $[11\bar{2}0]$  zone axis.

the more diffused  $B_{12}As_2$  spots are labeled with hexagonal  $hkil$  indices with subscripts of roman numerals I or II indicating matrix or a twin orientation (in some cases the matrix and twin reflections coincide). Although the film completely covers the substrate, the area of the  $B_{12}As_2$  diffraction spots appears different from that of the SiC spots due to the presence of mosaicity in the film. This leads to an overall divergence in the diffracted beams emanating from both the matrix and twin regions. The overall appearance of the  $B_{12}As_2$  matrix and twin diffraction spots is consistent with a mosaic and quite homogeneous solid solution of twin and matrix domains, which are of a size that is below the spatial resolution of x-ray topography (a few microns). This was corroborated by a scanning electron microscope (SEM) [see Fig. 2(b)], which reveals a composite structure comprising two types of equilateral triangular features, each with dimensions of several microns, which are mutually rotated by  $180^\circ$  about the surface normal in agreement with previous observations.<sup>1</sup> These triangular grains correspond to twin related  $B_{12}As_2$  domains. The morphology of the triangular features was determined using orientation information provided by SWBXT and found to consist of a flat  $(0001)_{B_{12}As_2}$  facet bounded by three equivalent  $(1\bar{1}00)_{B_{12}As_2}$  facets. Further microstructural information, in particular concerning the boundaries between

the various domains, was provided by conventional and HRTEM studies carried out on cross-sectional samples.

Conventional cross-sectional TEM observation along the  $[11\bar{2}0]$  zone axis [Fig. 3(a)] reveals a transition layer located between the film and the substrate. Figures 3(b) and 3(c) show selective area diffraction (SAD) patterns recorded from the  $B_{12}As_2$  film and the  $6H$ -SiC substrate respectively, confirming the epitaxial relationship determined from SWBXT. Compared to the epilayer and the substrate, the SAD pattern recorded from the transition layer shows relative disorder [see Fig. 4(a)]. Detailed simulation of Fig. 4(a), shown in Figs. 4(b)–4(d), reveals that the transition layer consists of an overlap of twinned  $B_{12}As_2$  domains with some strain. HRTEM was subsequently employed to provide information on the atomic configurations present in the various domains and the boundaries between them.

Figure 5(a) shows a HRTEM image recorded from a defect-free region of the film, viewed along  $[11\bar{2}0]$ . The origins of the various features observed on this image were investigated by comparing them to both the results of the multislice simulations [Fig. 5(b)]<sup>10</sup> and the projections of the crystal structure carried out using CARINE [Fig. 5(c)]. Multislice simulations carried out over a range of sample thicknesses and defocus values showed that good agreement can be found for sample thicknesses in the range of 8.6–12.0 nm with the best fit at 8.6 nm [Fig. 5(b)] and a defocus of 3 nm. Detailed comparison between the observed and simulated images and the CARINE projections indicates that the bright spots marked by the dotted circles in both experimental and simulated images as well as in the structural projection arise from neighboring B columns, while those marked by the solid circles arise from columns comprising As atoms and B atoms that project closest to them. Using a similar approach, the HRTEM of the transition layer and the subsequently grown region of the epilayer were used to investigate the detailed atomic configurations present in the various domains and in the various interfaces between them. In addition, the comparison of HRTEM images with models of the potential bonding configurations available at various nucleation sites on the  $(0001)$   $6H$ -SiC surface sheds considerable light on the nucleation and growth mechanisms of the  $B_{12}As_2$  film.

In the previously reported analysis of possible structural variants in this system (Michael *et al.*<sup>1</sup>), the choice of nucleation sites was based on alignment of threefold  $[0001]$  axes running through the centers of the icosahedra with various axes of the threefold symmetry on the SiC  $(0001)$  surface.

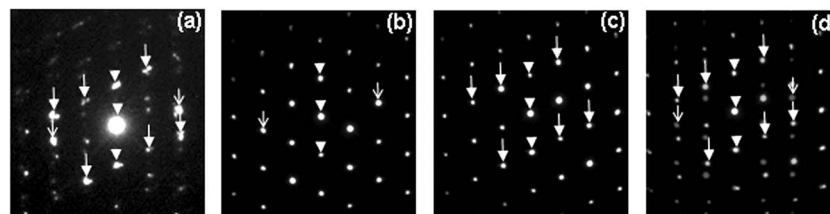


FIG. 4. (a) SAD pattern of the transition layer recorded along the  $[11\bar{2}0]$  zone axis. (b) Simulated SAD pattern of one of the  $B_{12}As_2$  twin domains. (c) Simulated SAD pattern of the other  $B_{12}As_2$  twin domains. (d) Simulated SAD pattern resulted from (b) and (c) showing an overlapped pattern of  $B_{12}As_2$  twinned domains. The spots indicated by  $\downarrow$  and  $\nabla$  represent diffraction spots from matrix and twin domains, respectively. The diffraction spots indicated by  $\blacktriangledown$  represent diffraction spots common to both matrix and twin.

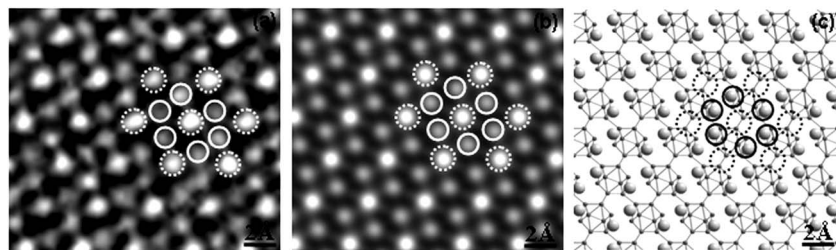


FIG. 5. (a) Experimental HRTEM image recorded from a defect-free region of the  $B_{12}As_2$  film viewed along  $[11\bar{2}0]$ . (b) Simulated HRTEM image of the  $B_{12}As_2$  film corresponding to (a) with defocus=3 nm and sample thickness=8.6 nm. (c) Atomic configuration of the  $B_{12}As_2$  structure with the same projection direction as (a).

While this approach provides the basic framework for selection of nucleation sites, we propose here that the number of possible nucleation sites be reduced compared to this analysis based on the consideration of possible bonding configurations between the epilayer and the substrate. If the  $B_{12}As_2$  adopts a  $(0001)$  orientation on the  $(0001)$  SiC substrate, it is instructive to consider the dangling bond configurations presented by the  $(000\bar{3})_{B_{12}As_2}$  planes toward the substrate surface, as shown in Fig. 6(a). The triangular configurations of boron atoms that constitute the lower ends of the icosahedra each present a triangular set of boron dangling bonds. These triangular configurations of boron atoms form a hexagonal network that can be accommodated on the substrate surface by the triangular Si dangling bond configurations presented at sites such as those labeled  $A_1$  in Fig. 6(b). Simultaneously, the As dangling bonds [one of which is also shown in Fig. 6(a)] can be accommodated by the Si dangling bonds that are located at the centers of those triangular configurations made up from  $A_1$  sites, which have their apexes pointing up [see Fig. 6(b)]. Since all dangling bonds on both the upper sub-

strate and lower epilayer surfaces are accommodated in this scheme, it appears that this is a highly plausible bonding configuration. For this same orientation of B triangle (i.e., with apex pointing up), there are three other possible sites, which allow similar bonding to Si atoms, shown in Fig. 6(a) as  $A_2$ ,  $A_3$ , and  $A_4$ , which are shifted by  $1/6\langle 11\bar{2}0 \rangle_{B_{12}As_2}$  from the  $A_1$  sites. These constitute translational variants. B triangles in twinned orientation (i.e., with apexes pointing down) can be bonded in a similar way to Si triangles on the four sites marked as  $A'_5$ ,  $A'_6$ ,  $A'_7$ , and  $A'_8$  in Fig. 6(b), which are shifted by multiples of  $1/12\langle 1\bar{1}00 \rangle_{B_{12}As_2}$  from the  $A_1$  sites. These make a total of eight distinct nucleation sites, a number smaller than that proposed by Michael *et al.*<sup>1</sup> This reduction in number of nucleation sites predicted by our modified model can be illustrated by considering, for example, the three so-called chemical variants proposed by Michael *et al.*,<sup>1</sup> which position the B triangles over Si, C, and interstice sites. Of these, according to our bonding analysis, only the interstice site can accommodate the three boron dan-

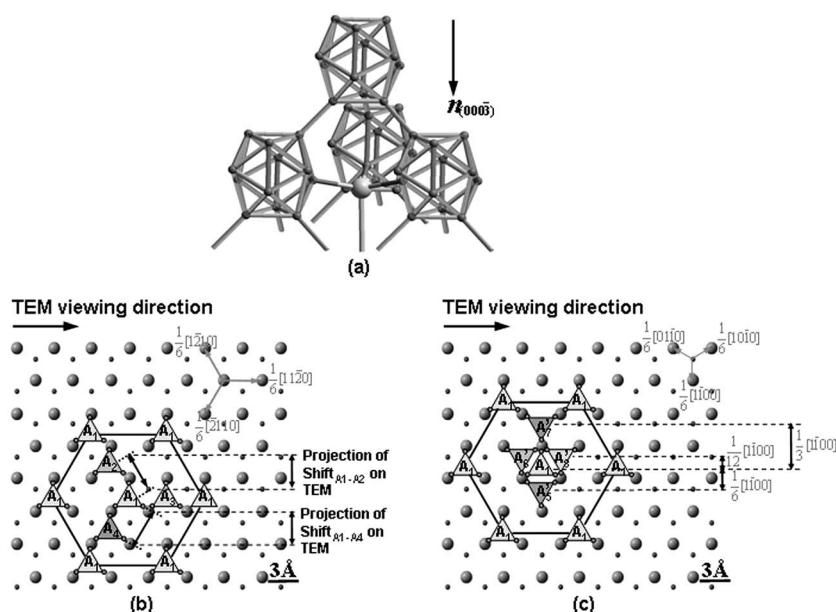


FIG. 6. (a) Schematic highlighting the dangling bond configurations presented by the  $(000\bar{3})_{B_{12}As_2}$  plane. Note the triangular configurations of boron dangling bonds at the lower ends of the icosahedra as well as the arsenic dangling bond. (b) Plan view of four possible translationally variant  $B_{12}As_2$  nucleation sites ( $A_1$ ,  $A_2$ ,  $A_3$ , and  $A_4$ ) on Si-face  $(0001)$   $6H$ -SiC. Si and C atoms are represented by large and small spheres, respectively. In each case, the sets of three B dangling bonds protruding from the B triangles form bonds to the Si atoms which also form a triangular configuration. Projections of the shifts observed via TEM are labeled; (c) Plan view of the four possible translationally variant nucleation sites ( $A'_5$ ,  $A'_6$ ,  $A'_7$ , and  $A'_8$ ) for  $B_{12}As_2$  in twinned orientations. The projections of possible shifts on TEM are marked as  $1/12[1\bar{1}00]$ ,  $1/6[1\bar{1}00]$ , and  $1/3[1\bar{1}00]$ , respectively.

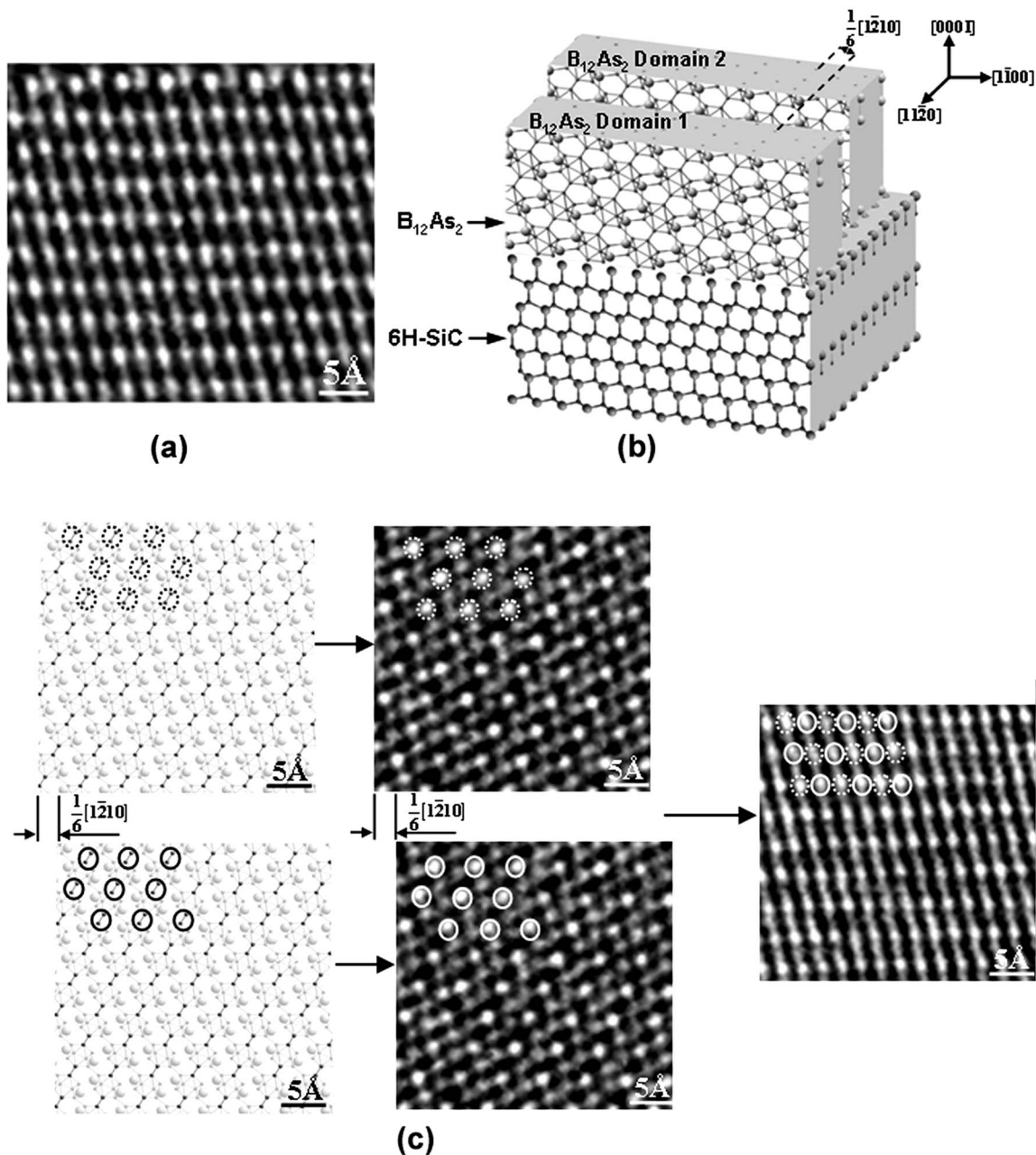


FIG. 7. (a) HRTEM observation of the transition layer viewed along the  $[11\bar{2}0]_{B_{12}As_2}$  zone axis. (b) Crystal visualization of translation variants with  $1/6[1\bar{2}10]$  mutual shift arising from nonequivalent nucleation sites on the substrate. (c) Moiré pattern formed by overlapping two  $B_{12}As_2$  HRTEM images taken along  $[11\bar{2}0]$  direction mutually shifted by  $1/6[1\bar{2}10]$  compared with CARINE projections. According to the HRTEM simulation in Fig. 5, the solid circles in Fig. 7(c) correspond to the projection of neighboring B columns from  $B_{12}As_2$  domain1, while the dotted circles correspond to those from domain2.

gling bonds presented at the lower end of the icosahedron as well as the As dangling bonds. At the Si site, the boron atom bonds are oriented toward the C atoms that are buried below the surface and have no dangling bonds. At the C site, the boron atom bonds are oriented toward the interstices between the Si atoms which can provide no bonds. Thus, Si and C chemical variants can be eliminated. In a similar way, imposing bonding restrictions on the rotational and translational variants depicted in Michael *et al.*<sup>1</sup> also reduces their numbers.

Since, according to our analysis, there are eight possible nucleation sites it is perhaps not surprising that there is some degree of disorder in the  $B_{12}As_2$  film close to the interface as

the islands that nucleate at these various sites coalesce and begin to overgrow each other. This is consistent with the conventional TEM observation of the  $\sim 200$  nm thick transition layer close to the interface (Fig. 3).

Direct evidence for the coexistence of the  $1/6\langle 11\bar{2}0 \rangle_{B_{12}As_2}$  translational variants of Fig. 6(b) can be found in the HRTEM images recorded from the transition layer region such as Fig. 7(a). The complex structure observed on this image suggests that it may be due to the overlap between more than one variant. This is confirmed by considering the overlap between two translational variants mutually shifted by a  $1/6[1\bar{2}10]_{B_{12}As_2}$  translation, as shown

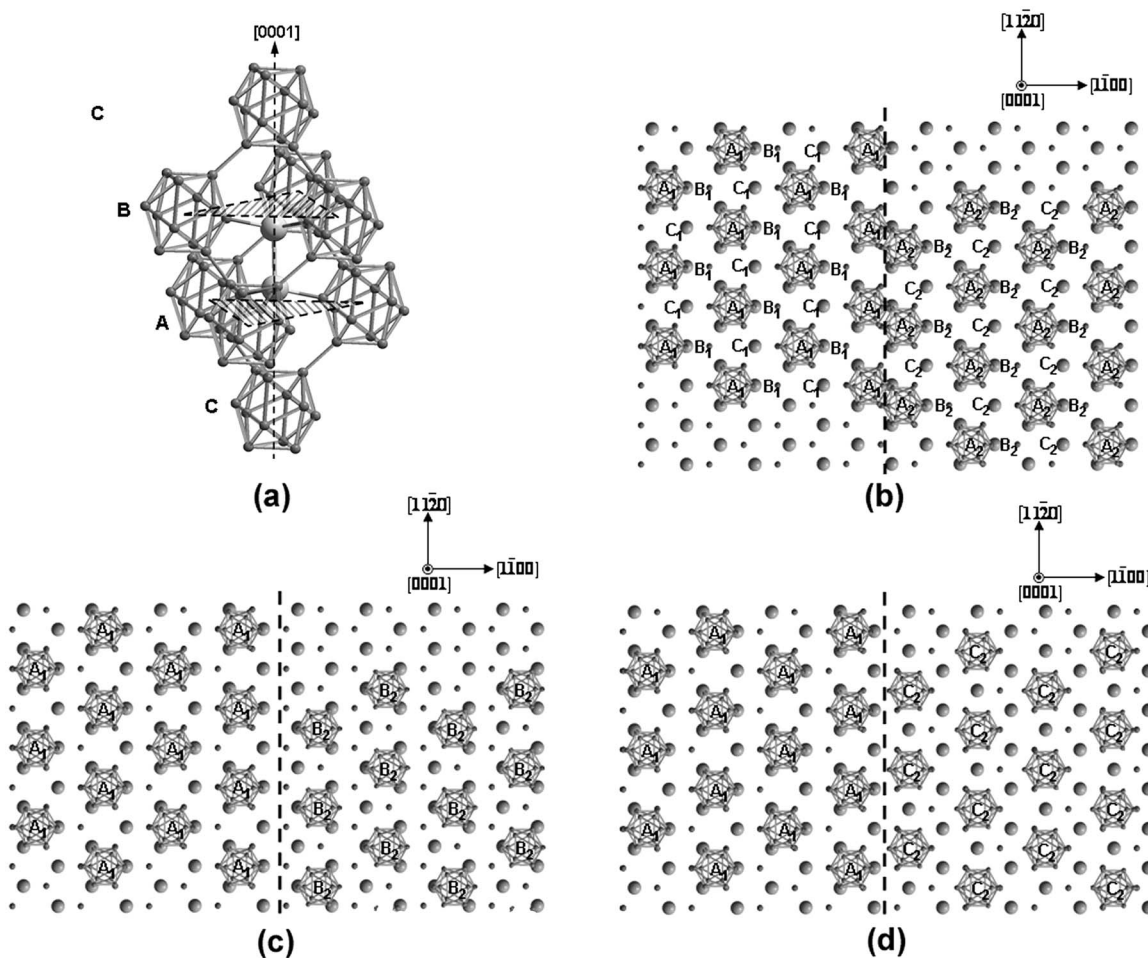


FIG. 8. (a) Representation of the structure of  $B_{12}As_2$  showing that it can be considered as a (0001) layered structure with the boron icosahedra forming equilateral triangular nets as represented by the stacking positions A (at the apexes of the shaded triangle in layer A). Successive layers adopt similar configurations with the boron icosahedra occupying the stacking positions B and C. (b) Projection of the stacking positions of the boron triangles on the (0001)<sub>SiC</sub> substrate surface. Left-hand side shows the boron triangles located at sites of type  $A_1$  [see Fig. 6] and the right-hand side shows boron triangles located at sites of type  $A_2$ . The stacking positions of the subsequently stacked layers  $B_1$  and  $C_1$  and  $B_2$  and  $C_2$  are also shown. The dotted line dividing the two regions schematically represents a lateral boundary between the translational domains which are mutually shifted by  $1/6[1\bar{2}10]$ . (c) Same region following a  $1/3[0001]$  shift of the right hand  $B_{12}As_2$  domain aligning  $A_1$  with  $B_2$  and enabling stable bonding between the two  $B_{12}As_2$  domains. (d) Same regions following an equivalent  $1/3[0001]$  shift of the right  $B_{12}As_2$  domain aligning  $A_1$  with  $C_2$  and again enabling equivalently stable bonding between the two  $B_{12}As_2$  domains.

in the CARINE model in Fig. 7(b). Further confirmation is provided by the Moiré pattern formed by the overlap, along the  $[1\bar{1}\bar{2}0]_{B_{12}As_2}$  electron imaging direction, between HRTEM images (recorded from a perfect  $B_{12}As_2$  region) mutually shifted by a  $1/6[1\bar{2}10]_{B_{12}As_2}$  translation, as shown in Fig. 7(c). Regions comprising overlapped translational variants were restricted to the transition layer with somewhat larger size domains of rotational variants dominating the film at thicknesses beyond  $\sim 200$  nm. In order to understand why and how the translational variants apparently grow out following around 200 nm of growth, it is instructive to consider the possible bonding configurations that might arise during the lateral coalescence of two translational variants.

In order to visualize this, it is useful to consider  $B_{12}As_2$  as a (0001) layered structure comprising the hexagonal networks of boron triangles, which are depicted in Fig. 6(b). If the first layer is accommodated at  $A_1$  sites, successive layers are accommodated at sites comprising stacking positions  $B_1$  and  $C_1$ , as shown schematically in perspective in Fig. 8(a)

and in projection on the left-hand side of Fig. 8(b). This ABC stacking sequence is somewhat analogous to that encountered in face-centered-cubic-type structures, although here the structure is not closely packed since, within a given layer (say,  $A_1$ ), the icosahedra are connected via bonds to arsenic atoms located at positions that project along [0001] to a second position (say,  $C_1$ ) in the stacking sequence. These arsenic atoms then connect along [0001] to other arsenic atoms in the same stacking position that connect triangular configurations of icosahedra in the third position (say,  $B_1$ ) in the stacking sequence. Thus,  $A_1$  and  $B_1$ ,  $B_1$  and  $C_1$ , and  $C_1$  and  $A_1$  layers are connected via arsenic atom pairs that are located, respectively, in the  $C_1$ ,  $A_1$ , and  $B_1$  stacking positions. For comparison purposes, the right-hand side of Fig. 8(b) shows the stacking sequence for one of the translational variants ( $A_2B_2C_2$ ). As these initially nucleated layers attempt to coalesce during growth, considerable bonding problems arise from the steric hindrance between boron icosahedra in the adjacent  $A_1$  and  $A_2$  stacking positions [see, for example, the

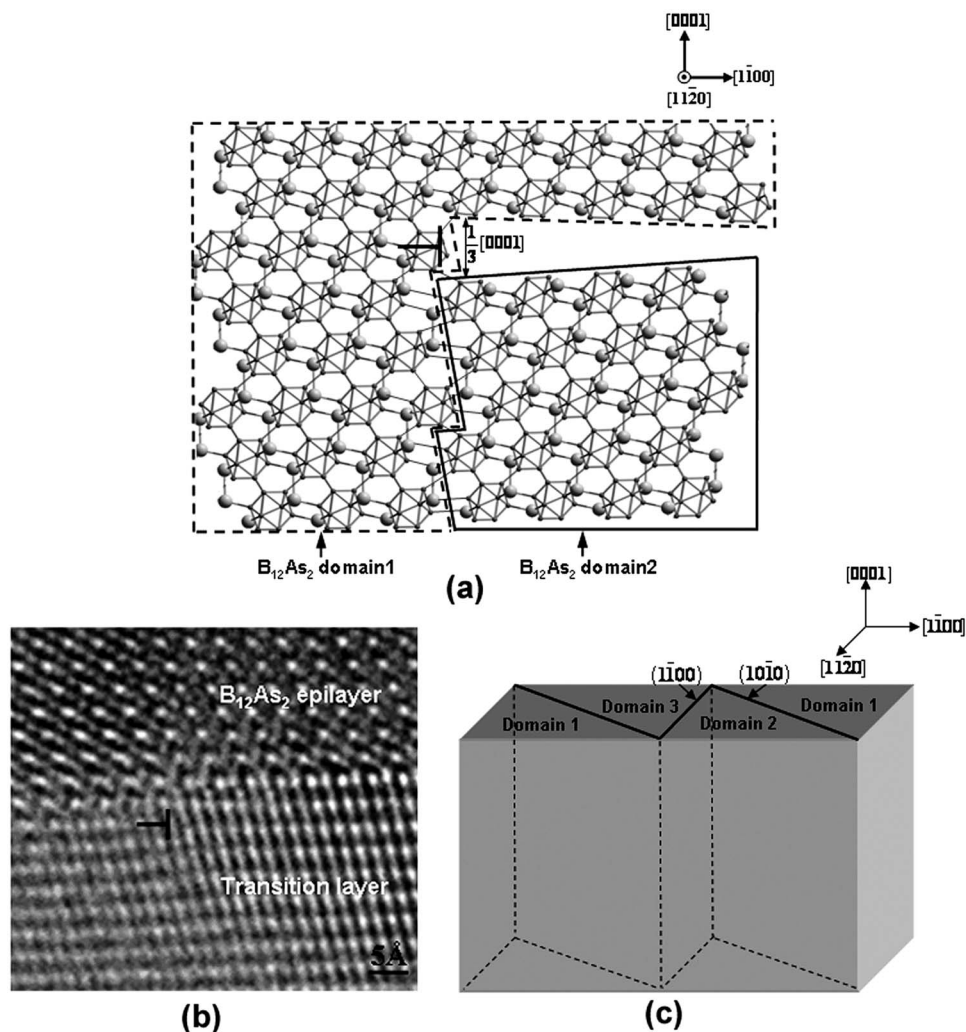


FIG. 9. (a) Crystal visualization, viewed along the  $[11\bar{2}0]$  electron imaging direction, showing how a Frank partial dislocation can produce the  $\frac{1}{3}[0001]$  shift. (b) HRTEM image recorded along  $[11\bar{2}0]$  zone axis showing a Frank partial dislocation in the interface between the transition layer and the  $B_{12}As_2$  epilayer at the junction between two translational variants. (c) Schematic of  $B_{12}As_2$  translational domain configuration, showing the possible domain configuration corresponding to Fig. 9(b).

interface schematically represented as a dashed line in Fig. 8(b)]. Similar problems occur in the lateral interfaces between the subsequently stacked  $B_1$  and  $B_2$  and  $C_1$  and  $C_2$  layers. Such problems can be ameliorated by shifting the structure of one of the variants by  $\frac{1}{3}[0001]$ , such that, for example,  $A_1$  becomes adjacent to  $B_2$  at the lateral interface [see Fig. 8(c)] or equivalently  $C_2$  [Fig. 8(d)]. Similar shifts are experienced in all subsequent layers, enabling the boron icosahedra (and the As atoms) to bond with each other in a much more stable configuration, albeit distorted. This  $\frac{1}{3}[0001]$  shift can be produced by the creation of a Frank partial dislocation with  $b=\frac{1}{3}[0001]$  that can be produced by the collapse of layers in one of the variants as they overgrow each other, as shown in Fig. 9(a). This provides the mechanism by which the translational variants can be effectively eliminated during growth. An example of such a Frank partial dislocation can be seen in the HRTEM image recorded from the transition region shown in Fig. 9(b). Figure 9(c) shows the postulated translational domain configuration.

While the creation of  $\frac{1}{3}[0001]_{B_{12}As_2}$  Frank partial dislocations enables the elimination of the translational variants, no such solution can be found for the bonding problems created by lateral coalescence of twin variants. These latter boundaries tend to be diffused and wavy and persist until one twin variant is able to overgrow the other, enabling the cre-

ation of much more stable (0003) twin boundaries. The existence of rotational variants in these films can actually be predicted from the theory of degenerate epitaxy, which treats the growth of a lower symmetry epitaxial film on a higher symmetry substrate.<sup>11,12</sup> This theory, which is based on two dimensional point group analysis of the substrate and epilayer surfaces, predicts the existence of two rotational variants for the growth of  $3m$  symmetry (0001)  $B_{12}As_2$  on  $6mm$  symmetry (0001)  $6H$ -SiC. These rotational variants are related by a symmetry operation that exists in the substrate but not in the film ( $\{1\bar{1}00\}$  mirror planes exist in both  $B_{12}As_2$  and  $6H$ -SiC while  $\{11\bar{2}0\}$  mirror planes exist only in  $6H$ -SiC).

While rotational variants are readily observable in HRTEM images, detailed observation of the atomic configurations across (0003) twin boundaries can provide verification of the twin nucleation sites on the SiC surface. Figure 10(a) shows a HRTEM image recorded from a region of the  $B_{12}As_2$  film close to the interface containing (0003) twin boundaries with the simulated images shown as insets. Figure 10(b) is the magnified image of the enframed dotted region in Fig. 10(a). If these boundaries originated from the overgrowth of a twinned island across an untwinned island, the shifts between the twin and matrix nucleation sites should manifest in the (0003) twin boundaries. The projected

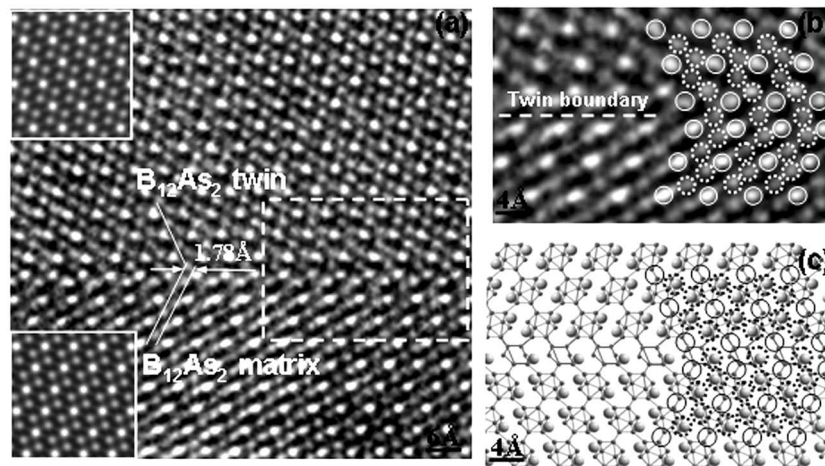


FIG. 10. (a) High resolution TEM image, taken along  $[11\bar{2}0]_{6H-SiC}$  zone axis, recorded from a defective region in the  $B_{12}As_2$  film containing (0003) twin boundaries with  $1/6[1\bar{1}00]_{B_{12}As_2}$  projected shift. The left two insets in (a) are the simulated  $B_{12}As_2$  HRTEM images for matrix and its twin with defocus = 3 nm and sample thickness = 8.6 nm. (b) Enlarged HRTEM image of the enframed dotted region in (a). (c) Corresponding crystal visualization to (b) showing the postulated atomic configuration across the (0003)  $B_{12}As_2$  twin boundaries. The solid circles stand for the projection of neighboring B columns, and the dotted ones for the projection of columns comprising As and their nearest B neighbors.

shifts in the twin planes along the TEM viewing direction would either be  $1/12[1\bar{1}00]_{B_{12}As_2}$ ,  $1/6[1\bar{1}00]_{B_{12}As_2}$ , or  $1/3[1\bar{1}00]_{B_{12}As_2}$ , as shown in Fig. 6(c). The twin boundaries shown in Fig. 10(a) exhibit a shift of around 1.78 Å, corresponding to  $1/6[1\bar{1}00]_{B_{12}As_2}$ , thus confirming the formation mechanism. Such shifts were commonly observed in twin boundaries throughout the film. These types of twin boundaries can be referred to as “faulted twin boundaries.” The detailed atomic and bonding configurations across such twin boundaries are discussed in the following.

In addition to providing information on the nucleation sites, HRTEM of the twin boundaries in comparison with CARINE structural projections enables the possible bonding configurations across the observed (0003) twin boundaries to be assessed. For the faulted twin boundaries exhibiting the  $1/6[1\bar{1}00]_{B_{12}As_2}$  shift, the structure proposed in Fig. 10(c)

maintains reasonable bonding and agrees well with the HRTEM observations. In this structure, boron forms nine atom clusters in the shape of a triaugmented triangular prism (one of the Johnson<sup>13</sup> figures, similar to the icosahedron). For those twinned domains nucleated on sites shifted by  $1/12[1\bar{1}00]_{B_{12}As_2}$  with respect to the matrix, as viewed along  $[11\bar{2}0]$ , the magnitude of this shift ( $\sim 0.9$  Å) would be difficult to discern on the HRTEM images. Twin boundaries exhibiting little or no shift are relatively uncommon in the film although an example of such twin boundaries is shown in Figs. 11(a) and 11(b) along with the suggested atomic configuration [Fig. 11(c)]. To maintain reasonable bonding, arsenic atoms in the  $B_{12}As_2$  matrix are directly bonded to arsenic atoms from the twin boron icosahedra from the matrix, and the twins are bonded to each other across the twin boundaries.

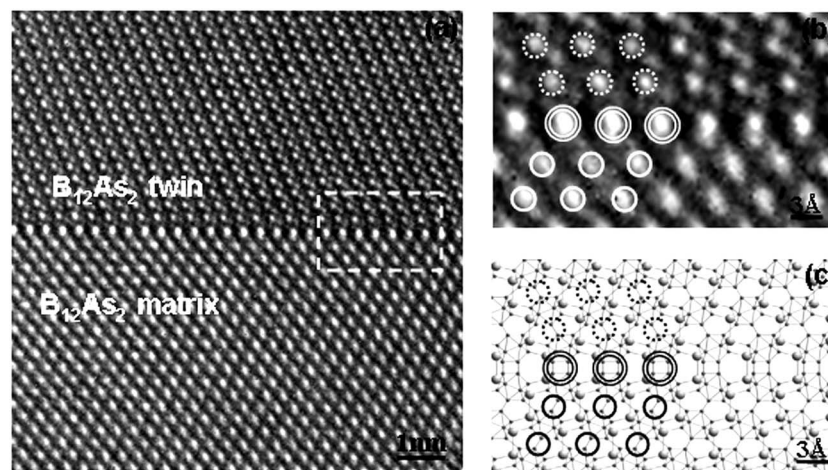


FIG. 11. (a) High resolution TEM image, taken along the  $[11\bar{2}0]_{6H-SiC}$  zone axis, recorded from another defective region in the  $B_{12}As_2$  film containing (0003) twin boundaries with  $1/12[1\bar{1}00]_{B_{12}As_2}$  projected shift. (b) Enlarged HRTEM image of the enframed dotted region in (a). (c) Crystal visualization corresponding to (b) showing the postulated atomic configuration across the (0003)  $B_{12}As_2$  twin boundaries. The dotted circles correspond to the projection of the neighboring B columns in the  $B_{12}As_2$  twin, the single solid circles to the projection of neighboring B columns in the  $B_{12}As_2$  matrix, and the double solid circles to the columns comprising bonded B atoms that make up the  $B_{12}As_2$  twin boundaries.



#### IV. CONCLUSIONS

The microstructure in  $B_{12}As_2$  epitaxial layers grown by CVD on (0001) 6H-SiC substrates has been analyzed in detail. SWBXT enabled macroscopic characterization of the substrate/epilayer ensembles and revealed the presence of a quite homogeneous solid solution of twin and matrix epilayer domains forming a submicron mosaic structure. The growth orientation of the epilayer with respect to the substrate was determined to be  $(0001)_{B_{12}As_2} \langle 11\bar{2}0 \rangle_{B_{12}As_2} \parallel (0001)_{6H-SiC} \langle 11\bar{2}0 \rangle_{6H-SiC}$ .  $B_{12}As_2$  twinned domains were found in the epilayer and the twin relationship consisted of a  $180^\circ$  (or equivalently  $60^\circ$ ) rotation about  $[0001]_{B_{12}As_2}$  in agreement with previous reports. A  $\sim 200$  nm thick disordered transition layer was revealed by cross-sectional HRTEM and was suggested to arise from the coalescence of translationally and rotationally variant domains nucleated at various nucleation sites on the (0001) 6H-SiC surface. Eight possible types of nucleation sites were found to be available on the substrate surface based on analysis of the stable bonding configurations between the boron triangles at the bottom of the boron icosahedra and the Si dangling bonds on the Si oriented (0001) 6H-SiC substrate surface. In the transition layer, competition between the growth of the various domains is mediated in part by the energy of the boundaries created between them as they coalesce. Boundaries between translationally variant domains are shown to have unfavorable high-energy bonding configurations, while the formation of a  $1/3[0001]_{B_{12}As_2}$  Frank partial dislocation enabled elimination of these high-energy boundaries during mutual overgrowth. Consequently the film quality beyond thicknesses of  $\sim 200$  nm can be improved as the translational variants grow out, leaving only the twin

variants. (0003) twin boundaries in the regions beyond 200 nm are shown to possess fault vectors such as  $1/6[1\bar{1}00]_{B_{12}As_2}$ , which are shown to originate from the mutual shift between the nucleation sites of the respective domains.

#### ACKNOWLEDGMENTS

The authors gratefully acknowledge the support of the National Science Foundation under Grant No. 0602875 and of the Engineering and Physical Science Research Council (EPSRC-GB) under Grant No. EP/D075033/1 under the NSF-EPSRC-GB Joint Materials Program. The x-ray topography experiments were carried out at the Stony Brook Topography Facility (Beamline X19C) at the National Synchrotron Light Source (NSLS), Brookhaven National Laboratory, which is supported by the U.S. Department of Energy (DOE) under Grant No. DE-AC02-76CH00016.

<sup>1</sup>J. R. Michael, T. L. Aselage, D. Emin, and P. G. Kotula, *J. Mater. Res.* **20**, 3004 (2005).

<sup>2</sup>D. Emin, *Phys. Today* **40**, 55 (1987).

<sup>3</sup>D. Emin, *J. Solid State Chem.* **179**, 2791 (2006).

<sup>4</sup>D. Emin and T. L. Aselage, *J. Appl. Phys.* **97**, 013529 (2005).

<sup>5</sup>D. Emin, *J. Solid State Chem.* **177**, 1619 (2004).

<sup>6</sup>M. Carrard, D. Emin, and L. Zuppiroli, *Phys. Rev. B* **51**, 11270 (1995).

<sup>7</sup>R. H. Wang, D. Zubia, T. O'Neil, D. Emin, T. Aselage, W. Zhang, and S. D. Hersee, *J. Electron. Mater.* **29**, 1304 (2000).

<sup>8</sup>W. M. Vetter, R. Nagarajan, J. H. Edgar, and M. Dudley, *Mater. Lett.* **58**, 1331 (2004).

<sup>9</sup>R. Nagarajan, Z. Xu, J. H. Edgar, F. Baig, J. Chaudhuri, Z. Rek, E. A. Payzant, H. M. Meyer, J. Pomeroy, and M. Kuball, *J. Cryst. Growth* **273**, 431 (2005).

<sup>10</sup>J. M. Cowley and A. F. Moodie, *Acta Crystallogr.* **10**, 609 (1957).

<sup>11</sup>C. P. Flynn and J. A. Eades, *Thin Solid Films* **389**, 116 (2001).

<sup>12</sup>S. W. Chan, *J. Phys. Chem. Solids* **55**, 1137 (1994).

<sup>13</sup>N. W. Johnson, *Can. J. Math.* **18**, 169 (1966).